

AMERICAN UNIVERSITY OF BEIRUT

QUANTIFYING AND MAPPING SALTWATER INTRUSION
IN A COMPLEX URBAN ENVIRONMENT: A UNIVERSAL
KRIGING APPROACH

by
KARIM TAREK KORBANE

A thesis
submitted in partial fulfillment of the requirements
for the degree of Master of Engineering
to the Department of Civil and Environmental Engineering
of the Maroun Semaan Faculty of Engineering and Architecture
at the American University of Beirut

Beirut, Lebanon
August 2020

AMERICAN UNIVERSITY OF BEIRUT


QUANTIFYING AND MAPPING SALTWATER INTRUSION
IN A COMPLEX URBAN ENVIRONMENT: A UNIVERSAL
KRIGING APPROACH

by

KARIM TAREK KORBANE

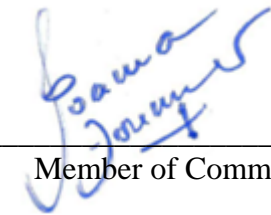
Approved by:

Dr. Ibrahim Alameddine, Assistant Professor
Department of Civil and Environmental Engineering, AUB



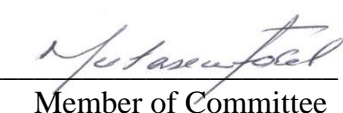
Advisor

Dr. Joanna Doummar, Assistant Professor
Department of Geology, AUB



Member of Committee

Dr. Mutasem El Fadel, Professor
Department of Civil and Environmental Engineering, AUB



Member of Committee

Date of thesis defense: August 28, 2020

AMERICAN UNIVERSITY OF BEIRUT

THESIS, DISSERTATION, PROJECT RELEASE FORM

Student Name:

_____Korbane_____Karim_____Tarek_____

Last

First

Middle

Master's Thesis Master's Project Doctoral Dissertation

I authorize the American University of Beirut to: (a) reproduce hard or electronic copies of my thesis, dissertation, or project; (b) include such copies in the archives and digital repositories of the University; and (c) make freely available such copies to third parties for research or educational purposes.

I authorize the American University of Beirut, to: (a) reproduce hard or electronic copies of it; (b) include such copies in the archives and digital repositories of the University; and (c) make freely available such copies to third parties for research or educational purposes after:

One ---- year from the date of submission of my thesis, dissertation, or project.

Two ---- years from the date of submission of my thesis, dissertation, or project

Three -x- years from the date of submission of my thesis, dissertation, or project.



16/09/2020

Signature

Date

ACKNOWLEDGMENTS

First of all, I would like to express my sincere gratitude to my advisor, Dr. Ibrahim Alameddine, whose knowledge, guidance, insights, and motivation were irreplaceable in developing this 2-year long work. I would also like to thank Dr. Joanna Doummar for sharing her valuable knowledge and experience in the field of hydro-geology, and Dr. Mutasem El-Fadel for his constructive feedback, expertise, and providing me with the opportunity to pursue this work.

I am grateful to Eng. Mohammad Tabsh, the General Manager of Mahmoud Tabsh Engineering and Trading SARL, for sharing his company's valuable expertise on well drilling in Beirut. The data that he provided was instrumental towards pushing this research forward. I would also like to acknowledge the help I received from Eng. Habib Asmar from the "Beirut and Mount Lebanon Water Establishment". I also would like to thank Dr. Ramez Zayyat for his guidance throughout the required laboratory work at the Environmental Engineering Research Center (EERC). Many thanks are extended to the Beirut Urban Lab at AUB for providing some of the funding needed to monitor salinity levels in Beirut and for sharing some of the necessary GIS data used in this project. I would also like to express my gratitude to the AUB University Research Board for covering the costs associated with the extensive field work conducted in this study.

Last but not least, I remain forever grateful to my father, mother, and brother for their continuous moral support, without which I would not have made it throughout. Many thanks to my friends, who have made the time spent at AUB truly unforgettable. Last but not least, my warmest thanks go to my precious lady and number one supporter, for never ceasing to be by my side and always pushing me to do my absolute best.

AN ABSTRACT OF THE THESIS OF

Karim Tarek Korbane for Master of Engineering
Major: Environmental and Water Resources Engineering

Title: Quantifying and Mapping Saltwater Intrusion in a Complex Urban Environment: A Universal Kriging Approach

Unsustainable groundwater exploitation in coastal aquifers has resulted in significant drops in freshwater heads and the promotion of seawater intrusion (SWI) into affected coastal aquifers. With nearly two-thirds of the world's population living in coastal cities, SWI is a global problem impacting many coastal aquifers worldwide. Several modelling frameworks have been developed over the years and implemented for mapping SWI; yet they have performed poorly in complex urban heterogeneous karst environments with limited data. In the current study, a Universal Kriging (UK) model is proposed and developed for the city of Beirut, Lebanon. The developed model was successfully able to capture the main socio-economical, geological/geographical, and land-use drivers of SWI in the study area, while at the same time explaining the spatial correlation structure in the sampled data. The developed UK outperformed a landuse regression (LUR) model across a set of selected model performance metrics (NSE 0.71 vs 0.54; RMSE 0.44 vs 0.93), while at the same time significantly reducing prediction uncertainties across the spatial domain by more than 20 %. Moreover, model validation results showed that both the UK and LUR models were significantly more robust and showed higher prediction skills as compared to previously developed kriging and GIS-based groundwater vulnerability models for the same study area. Overall, the predictive maps generated from the UK model clearly highlighted the severity of SWI in Beirut, whereby more than 55% of the groundwater aquifer in the city was predicted to hold brackish to saline waters. The model results also showed clear large-scale and fine-scale spatial variabilities in the predicted salinity levels, while also identifying regions suffering from upconing and those that appear to be benefiting from potential freshwater karst conduits or from local elevated recharge rates. The results of this study provide a promising modelling and mapping approach that can be implemented to map SWI in other poorly monitored urban coastal aquifers and to better understand their vulnerabilities to anthropogenic stressors.

CONTENTS

ACKNOWLEDGMENTS.....	1
ABSTRACT	2
LIST OF ILLUSTRATIONS	4
LIST OF TABLES	5
CHAPTER I: INTRODUCTION.....	5
CHAPTER II: MATERIALS AND METHODS.....	6
A. Study area.....	11
B. Sample collection and laboratory testing	14
C. Model development.....	15
1. Landuse regression model	15
2. Universal kriging model	21
3. Model comparison and SWI mapping.....	23
CHAPTER III: RESULTS AND DISCUSSION.....	25
A. Saltwater intrusion in the Beirut Aquifer	25
B. SWI model predictions and performance.....	28
CHAPTER IV- CONCLUSIONS.....	38
REFERENCES	41

ILLUSTRATIONS

Figure	Page
1. Geographic location of study area	12
2. Sampled wells in first and second rounds across the city of Beirut	15
3. Categorization of study area into geologically protected vs. unprotected zones, based on frequency of freshwater supply, and recent vs. old urbanization areas	19
4. Measured TDS and chloride levels during the sampling campaign of 2018-2019... ..	26
5. TDS levels across the different administrative zones of Beirut.....	26
6. Variation of observed TDS as a function of frequency of fresh water supply and the presence of geological protection	27
7. Variation of measured TDS levels as a function of distance to coastline.....	27
8. Predicted salinity level status of groundwater as a function of well depth for the Land Use Regression (LUR) model and the Universal Kriging (UK) model	31
9. Predicted salinity levels as a function of depth.....	33
10. Predicted TDS levels along two cross-sections at a depth of 150 m.	35
11. Predicted versus observed log(TDS) levels for the LUR model and the UK model	36
12. Log(TDS) prediction variances at a depth of 100 m for LUR predictions and UK predictions.....	36

TABLES

Table	Page
1. Proposed predictors for the SWI LUR model.....	18
2. Model performance statistics	24
3. Developed LUR model for predicting log(TDS)	30
4. Leave-one-out cross-validation (LOOCV) based statistics for three semi-variogram UK models	32

CHAPTER I

INTRODUCTION

Increased pressure on the world's freshwater resources has had major negative impacts on the socio-economic well-being of many communities as well as on the environment. Nearly 1.8 billion people (around 30% of the world's population) currently live in areas facing severe water stresses for at least six months per year, with fresh water withdrawals exceeding 75% of natural river flows (Heather et al. 2014). An additional 1.6 billion people live in areas facing economic water scarcity, where water is available but is limited due to inadequate infrastructure (Heather et al. 2014, Mekonnen and Hoekstra 2016, Roson and Damania 2017). Pressures on the available water resources will likely exacerbate in the future due to the projected population growth, climate change, alternations in the water cycle, expansion of irrigated agriculture, economic development, and increased frequency of droughts (Dai et al. 2019, Famiglietti 2014, Foulon and Rousseau 2019, Green 2016, Heather et al. 2014, Pittock et al. 2016, Zhang et al. 2017). In the face of chronic surface water shortages, many communities have resorted to the exploitation of groundwater resources, whose extraction costs have significantly decreased with time (Heather et al. 2014). As a result, the volume of groundwater withdrawals has tripled over the past 50 years (UN 2012) .

It is estimated that groundwater sources currently supplies approximately 20% of the world's water needs. It provides for 20% of the irrigation needs, 40% of the total industrial water withdrawals, and 50% of the municipal water demands (Zekster and Everett 2004). Despite its critical importance, few efforts have been put into place to

protect it; as a result, its management and monitoring remain relatively weak and fragmented, when compared to surface water resources (Famiglietti 2014, Jakeman et al. 2016). This has resulted in unsustainable groundwater exploitation across many parts of the world (Naderi 2020, Taniguchi et al. 2010). This overexploitation has caused stream-flow depletion, drops in the water table, loss of springs and wetlands, and the promotion of seawater intrusion (SWI) (Chang et al. 2011, Flores et al. 2020, Mancuso et al. 2020).

SWI is defined as the encroachment of saltwater inland as a result of declining freshwater heads and changes in the hydraulic gradient at the coastline (Barlow and Reichard 2010, Bruington 1972, Meyer et al. 2019, Watson et al. 2010). SWI is currently a major problem affecting many coastal aquifers worldwide (Dentoni et al. 2015, Huang and Chiu 2018, Lal and Datta 2019, Nishikawa et al. 2009, Romanazzi et al. 2015, Safi 2019, Shi and Jiao 2014, Werner 2010). With around two thirds of the world's population living in coastal cities (Singh 2014), improving our understanding of the relative contributions of the main drivers of SWI remains a high priority.

Several approaches have been developed over the years to quantify the main drivers of SWI and to model its development in space and time. These efforts can be divided into four main categories, namely: 1) mathematical SWI models that include the variable density flow/solute transport models (Chang et al. 2011, Giambastiani et al. 2007, Kerrou et al. 2010b, Langevin and Zygnerski 2013, Masterson and Garabedian 2007, Sanford and Pope 2010) and the sharp-interface models (Akbarpour and Niksokhan 2018, Beebe et al. 2016, Deng et al. 2017, Gorgij and Moghaddam 2016,

Mantoglou 2003, Mehdizadeh et al. 2015, Morgan et al. 2015, Ranjan et al. 2006, Uddameri et al. 2014); 2) geo-statistical models (Momejian et al. 2019b, Murgulet and Tick 2008); 3) groundwater vulnerability assessment models (Elewa et al. 2013, Lobo-Ferreira et al. 2005, Mahesha et al. 2012, Tomaszkiwicz et al. 2014, Trabelsi et al. 2016); and 4) geo-physical models (Cimino et al. 2008, Kura et al. 2014). All four methods have limitations, when it comes to capturing small-scale salinity variability in complex urban environments with limited hydrogeological data and a highly heterogeneous coastal karst aquifers. The hydraulic properties in karstic aquifers are known to vary considerably over small distances (Dubois et al. 2019). Fractures in the karst can affect the flow of seawater inland in several ways, including promoting the mixing zone width in the presence of vertical fractures in the vicinity of the seawater or pushing the saltwater-freshwater wedge seaward when horizontal fractures are present in the deep parts of the aquifer (Sebben et al. 2015). The sharp-interface models, for instance, have proven to be useful when regional estimates of the saltwater-freshwater interface are required (Reilly and Goodman 1985); yet they are unable to accurately predict groundwater salinity at the well level. On the other hand, the variable-density models have proven to be very sensitive to the uncertainties in the hydraulic conductivity fields (Safi 2019) and thus tend to be unsuitable for modelling highly heterogeneous coastal aquifers with limited hydrogeological data. Meanwhile, the complexity of the variable density models along with their high computational power requirements and numerical convergence problems hinder their effective use to model SWI at fine spatial scales (Kerrou et al. 2013, Kerrou et al. 2010a, Langevin and Zygnerski 2013, Sanford and Pope 2010). Moreover, groundwater vulnerability assessment models are only able to capture the overall aquifer vulnerability, with some

models (e.g. DRASTIC and EPIK) not inadequately accounting for the lateral movement of pollution (Metni et al. 2004, Momejian et al. 2019b). Additionally, both the geo-statistical and groundwater vulnerability assessment models have been shown to have limited capabilities to account for the small-scale salinity variations in highly heterogeneous karst urban coastal aquifers (Metni et al. 2004, Momejian et al. 2019b).

In light of the above, we propose a new SWI modelling approach that aims to capture the small-scale variability of salinity levels in a highly heterogeneous aquifer located beneath a complex urban coastal environment with limited hydrogeological data. This study adopts a technique that combines the strengths of land-use regression (LUR) models and geo-statistics in a modelling procedure that is termed Universal Kriging (UK). The method consists of incorporating a LUR model that accounts for the socio-economical, geological/geographical, and land-use drivers of SWI, while concurrently accounting for spatial autocorrelations in the sampled data. While both the LUR and UK have been successfully used to model environmental systems, such as ambient air quality (de Hoogh et al. 2013, Eeftens et al. 2012, Hoek et al. 2011, Ma et al. 2019, Wang et al. 2012, Xu et al. 2019, Young et al. 2016, Zalzal et al. 2020) and groundwater level fluctuations (Ahmadi and Sedghamiz 2006, Gundogdu and Guney 2007, Kumar 2007, Xiao et al. 2016), they have not been widely used to predict and map the spatial variations of groundwater quality in general and SWI specifically. This study is the first of its kind to apply UK in SWI predictions in a karst environment using groundwater salinity data collected from the coastal city of Beirut, Lebanon. It is hoped that this study will provide an opportunity to enhance our knowledge of the relative impact of different SWI drivers on salinity levels in data-scarce coastal cities with

heterogeneous aquifers. Moreover, the proposed methodology provides a mechanism towards the generation of salinity maps at a fine spatial resolution that can be used to identify SWI affected regions and isolate areas with high model uncertainties.

CHAPTER II

MATERIALS AND METHODS

A- Study area

The study area comprises the administrative boundaries of Beirut, the capital city of Lebanon. Beirut is located along the Eastern Mediterranean coastline (Figure 1). The city is bounded by the Mediterranean Sea from the North and West and the Beirut River to the East. The city extends over an area of about 20 km² and has a population density of about 18,000 inhabitants/km² (CAS 2009). It is administratively divided into 10 areas, namely: Ain-Mreisseh, Moussaytbeh, Mazraa, Bachoura, Zkak-el-Blatt, Ras-Beirut, Achrafiyeh, Remeil, Saifi, and Medawar. Topographically, the study area is relatively flat, with elevations ranging between 0 m adjacent to the sea up to 60 m in the Achrafiyeh area and along the south-western corner of Mazraa. The area is characterized by a dense urban fabric, covering around 70% of the city, with scattered shrublands, parks, vacant lands, and industrial zones occupying the remaining 30% (CNRS 2010).

The exposed geological formations in Beirut belong to the Cretaceous, Quaternary, and Tertiary ages (Peltekian 1980). The cretaceous and tertiary formations are mostly exposed in the North-Western and North-Eastern sections of the study area, respectively. The cretaceous formations, whose aquifers are characterized by high transmissivity but low storage capacity, are divided into three layers based on their ages: C4a, C4b, and C4c. The C4a layer is the oldest and has a thickness of about 200 m and is classified as an aquifer. The C4b layer, which has a thickness of about 125 m, is classified as an aquiclude. The topmost layer is the C4c layer; it has a thickness of about



Figure 1: Geographic location of study area

180 m and is classified as an aquifer (Walley 1997). The exposed geological formations for the rest of the study area are Quaternary. Quaternary deposits are characterized by alluvial, beach, and eolian deposits. They rest unconformably on the cretaceous fractured limestone. Quaternary deposits have a thickness of about 50 m and are classified as homogenous porous aquifers locally. Based on collected information on pumping depths, expert elicitation with local well drilling companies, as well as the analysis of geological cross sections in the study area, it is apparent that all sampled domestic wells in the city were tapping into the C4c cretaceous limestone layer. Few old shallow wells (~ 10m depth) in the city are known to tap into the quaternary aquifer; but none were sampled in this work.

Public water delivery in the study area faces several challenges related to chronic deficits, lack of metering, unsustainable water resource management, and weak governance. Moreover, the uneven temporal distribution of precipitation and the presence of a long dry season, typical of Mediterranean climates, have exacerbated water stress and complicated its management (Bou-Zeid and El-Fadel 2002, Roson and Damania 2017). As a result, water delivery through the public network covers only half the required demand (MoE and UNDP 2011). Water distribution in the city shows clear geographical differences, with some regions of Beirut receiving less than seven hours per day of fresh water supply, while others receive almost a continuous supply (Alameddine et al. 2018, EBML 2019, El-Fadel et al. 2003). In an effort to compensate for the resulting deficit, many households in the city have resorted to the illegal drilling of groundwater wells that operate without oversight and beyond safe yields (Imad 2003). The combination of the aquifer's intrinsic geological vulnerability, the city's chronic water deficits, and weak governance has resulted in the Beirut aquifer being the most severely affected coastal aquifer by SWI across Lebanon (MoEW and UNDP 2014). It has also been identified amongst the two most affected aquifers by SWI across the entire Eastern Mediterranean coastline (Rachid 2020).

SWI in the city was first recorded back in 1969 through geo-electrical measurements (FAO 1997). Since then, the groundwater chloride concentrations have continuously increased, reaching up to 4,200 mg/L in the year 2005 (Saadeh 2008). More recent field investigations carried out between 2013 and 2014 have shown that the Total Dissolved Solids (TDS) and chloride concentrations exceeded 20,000 mg/L and 10,000 mg/L respectively, in some zones of the study area (El-Fadel et al. 2014).

Several attempts have been carried out to characterize and model the vulnerability of the Beirut aquifer to SWI, including the development of geostatistical (Momejian et al. 2019b), vulnerability-based (Metni et al. 2004, Momejian et al. 2019b), and variable density flow/solute transport (Safi 2019) models. Yet, all of the developed models showed poor performance when validated with field data. Moreover, their salinity predictions were associated with high levels of uncertainties caused by the complexity of the aquifer and data scarcity.

B- Sample collection and laboratory testing

Water quality data were collected over two rounds (Figure 2). The first campaign took place between September 2018 and January 2019. In that round, a total of 132 water samples were collected from randomly selected buildings across Beirut. However, the sampled wells lacked accurate information on their depths. Thus, a second campaign of sampling targeted 65 wells with well-documented depths. That campaign spanned between August 2019 and October 2019.

All water samples were extracted using plastic sterile containers and placed in a cooler filled with ice bags before being transported to the Environmental Engineering Research Laboratory at the American University of Beirut, where testing for salinity took place. TDS levels were determined using a Eutech CyberScan CON 11 conductivity/TDS meter that has a measurement range of 0 to 99.9 ppt, a resolution of 0.05% over the entire measurement scale, and an accuracy of $\pm 1\%$. Prior to any measurement, the meter was calibrated with three standard conductivity calibration solutions, namely: 1143 $\mu\text{S}/\text{cm}$, 12.88 mS/cm , and 111.8 mS/cm . Chloride ion

concentrations were measured using the Mohr titration procedure according to ISO 9297:1989 by titrating the diluted sample with a 0.1 M AgNO_3 solution in the presence of 1 mL of a 5% K_2CrO_4 solution as an indicator. Both TDS and Chloride ions concentration are good indicators of groundwater salinity (Langevin and Zygnerski 2013, Sanford and Pope 2010).

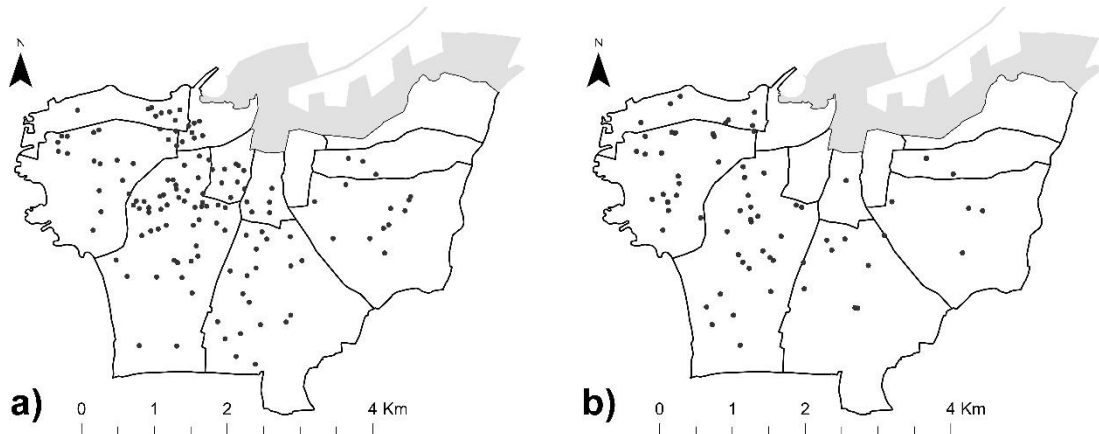


Figure 2: Sampled wells in a) first and b) second rounds across the city of Beirut. The greyed areas represent the port and the Beirut central district that have few residential buildings and largely sit on reclaimed land.

C- Model development

1- Landuse regression model

A LUR model was first developed to establish an empirical relationship between the measured salinity levels (TDS or chlorides) on one hand and a set of predefined predictors on the other. The predictor variables were selected based on previous studies and our understanding of the main physical drivers of SWI (Table 1). These drivers were divided into three main categories, namely 1) geological/geographical, 2) socio-economic, and 3) land-use based predictors.

The selected geological/geographical factors that affect groundwater salinity included pumping depth, distance to sea, elevation, the locations of faults, as well as the physical characteristics of the aquifer materials (Gorelick and Zheng 2015, Kourgialas et al. 2016, Lobo-Ferreira et al. 2005, Meyer et al. 2019, Yu and Michael 2019). We expect that as pumping depths increase or when the distance to the coastline decreases, the probability of tapping into saline water would increase (Herzberg 1901). Meanwhile, we expect that areas with higher elevations will experience less SWI. The proximity of a well to a fault may either exacerbate SWI through establishing preferential flow-paths for seawater or hinder SWI by providing preferential fresh-water flow-paths at certain locations or obstructing existing seawater pathways (Allen et al. 2002). In an effort to account for the potential impacts of fault lines, the Euclidean distance separating each sampled well from the nearest fault in the study area was calculated using the Spatial Analyst toolbox in ArcMap 10.6.2 (ESRI 2018). Similarly, the Euclidean distances between the wells and the coastline were determined. An in-depth analysis of the physical characteristics and spatial distribution of the aquifer material was conducted by studying different geological cross sections in the study area. Different geological cross-sections of the city were developed by relying on the geological outcrop and fault maps of Beirut (Dubertret 1955) along with a 10 m resolution Digital Elevation Model (DEM) map of the study area. The geological cross-sections showed the existence of a 70 m to 100 m thick C6 geological layer characterized by impermeable marls beneath the shoreline along the eastern parts of the city (from the Saifi region to Medawar; Figure 1 and Figure 3). This thick geological barrier is expected to hinder the advancement of SWI further inland. This layer appears to have been eroded over time in the other western sections of the city. The potential

impact of this protective layer in the model was accounted for by creating a binary categorical variable (“Geologically protected zone” versus “Geologically unprotected Zone”; Figure 3).

The anthropogenic predictors that can potentially promote SWI were divided into socio-economic and land-use-based drivers. The socioeconomic drivers tend to dictate groundwater abstraction rates (Klassen and Allen 2017), while changes in the land use and land cover have an effect on the direct recharge of the aquifer (Bhattachan et al. 2018, Deng et al. 2017, Uddameri et al. 2014). Given the lack of metering on the volume of water being pumped from the wells, groundwater abstraction rates were estimated through a set of surrogate variables. These included the number of buildings, the proliferation of small-scale water desalination units, and the presence of large commercial water pumping activities (i.e., gas and car wash stations, laundry services, hotels, and hospitals) within a set of spatial buffers defined around the wells. The GIS data was supplied by the Beirut Urban Lab (2020). The radii of the buffers were pre-defined to range between 10 m and 1 Km. Other indirect socio-economic variables affecting groundwater abstraction rates were also investigated. These included apartment prices ($\$/\text{m}^2$ for first floor unit) (RAMCO 2014) to account for increased water consumption with affluence (Hussien et al. 2016) as well as the frequency of fresh water supply from the public network. The frequency of water delivery through the public water supply network in Beirut for 2019 was obtained from the Beirut and Mount Lebanon Water Establishment (EBML 2019). As can be seen in Figure 3, the water delivery schedule for the city showed a clear spatial pattern that divided the city into two regions. The first zone is comprised of the western sections of the city and includes

Table 1: Proposed predictors for the SWI LUR model

Category	Possible Predictors	Description	Source of Information
Category #1: Geological/ Geographical Predictors	Geological protection against SWI	Categorical variable: “protected” and “unprotected”	Geological outcrop map (Dubertret, 1955) and DEM
	Well depth	Continuous variable (in m)	Data from well drilling companies
	Nearest Distance to sea	Continuous variable (in m)	Geological outcrop map (Dubertret, 1955)
	Distance to nearest fault	Continuous variable (in m)	GIS analysis
	Elevation	Continuous variable (in m)	DEM of Beirut, and GIS analysis
Category #2: Anthropogenic: Socio-Economic Predictors	Price of 1 square meter of a first floor apartment	Continuous variable (in \$/m ²)	(RAMCO, 2014)
	Frequency of freshwater supply from EBML	Categorical variable: zones with limited supply (<8hrs/day) and zones with continuous supply (>21 hrs/day)	(EBML, 2019)
Category #3: Anthropogenic: Land-use based predictors	# of buildings within a set of pre-defined buffers ¹ at each sampled location	Continuous variable	Field survey and GIS analysis
	Potential recharge zones (vacant or green areas) within a set of pre-defined buffers ¹	Continuous variable, expressed as % of total buffer area	LULC map, Google imagery, and GIS analysis
	Number of commercial water users within a set of pre-defined buffers ¹	Continuous variable	Google maps and GIS analysis
	Number of buildings with a desalination unit within a pre-defined set of buffers ¹	Continuous variable	Field survey and GIS analysis
	Land-use change over time	Categorical variable: “recently urbanized areas” and “old urbanized areas”	Comparison between aerial and satellite images

¹ buffer distances included 10 m, 25 m, 50 m, 75 m, 100 m, 200 m, 300 m, 400 m, 500 m, 750 m, 1000 m

the areas of Ras Beirut, Ain Mreisseh, Mina Al Hosn, Bachoura, Zkak el Blatt, Mazraa, and Moussaytbeh. Those areas received on average less than 8 hours/day of freshwater supply. The eastern parts of the city that included the areas of Achrafieh, Remeil, Saifi, and Medawar received more than 21 hours/day of freshwater supply. This large disparity in water distribution frequency between these two regions is largely related to inadequate storage and transmission infrastructure in the western sections of the city. The frequency of public water supply was accounted for in the LUR model

by developing a spatial categorical variable. Note that there is a large overlap between the geologically protected zone and the region with ample freshwater supply (Figure 3).

Finally, changes in the land-use and building density in the study area were assessed over the past 70 years through a comparison of aerial images taken in the 1950s (Lebanese Army 1950) with 2020 Landsat-8 images (USGS 2020). The comparison showed that large sections of the city were already urbanized in the 1950s. Only the south-western section of the city appears to have been undeveloped in the 1950s. That section experienced fast urbanization starting in the late 1990s and since then has become densely built. Since saltwater encroachment is a slow process that requires time to build up (Langevin and Zygnerski 2013, Sanford and Pope 2010), newly urbanized sections of the city (Figure 3) may experience a less pronounced saltwater wedge in comparison to older neighbourhoods that potentially had a longer pumping period. In an effort to account for the potential impact of local recharge on SWI, the percentage of pervious areas within pre-defined buffer zones (radii ranging from 10 m and 1 Km) were determined from recent 2020 Landsat-8 images (USGS 2020).

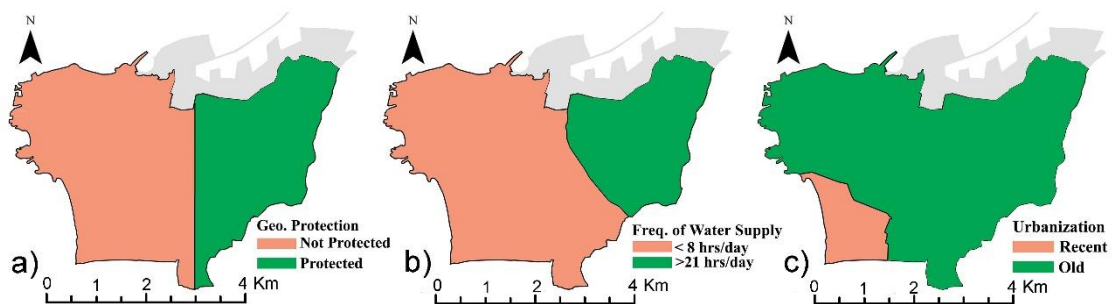


Figure 3: Categorization of study area into a) geologically protected vs. unprotected zones b) based on frequency of freshwater supply and c) recent vs. old urbanization areas

It should be noted that several other factors such as sea-level rise and climate change are well-known drivers of SWI (Akbarpour and Niksokhan 2018, Deng et al. 2017, Langevin and Zygnerski 2013, Masterson and Garabedian 2007). Yet, their impacts tend to be minor, when compared to the geological and anthropogenic drivers in the case of Beirut (Safi 2019), and largely uniform across the city. As such, they were not accounted for in this study.

The LUR model selection process was conducted using the R software (R Core Team 2018). Models were developed using the bi-directional elimination stepwise regression analysis using the entire set of the pre-defined predictors (Table 1). The final model was chosen based on having the lowest Akaike’s Information Criterion (AIC) (Akaike 1974), while ensuring that only statistically significant predictors (90% confidence interval) were kept in the model. Statistically significant predictors were also analysed so as to ensure that they were in agreement with our understanding of the SWI phenomenon and that the model did not suffer from multi-collinearity. The model’s performance was evaluated based on its R^2 , the Nash-Sutcliffe Efficiency (NSE) coefficient (Nash and Sutcliffe 1970), percent bias (PBIAS) and Residual Standard Deviation (RSD), while its robustness was tested using cross validation. The LUR model structure is shown in Equation 1:

$$\log(TDS) [\mathbf{r}] = \sum_{i=1}^n a_n f_n(\mathbf{r}) + \varepsilon \quad (\text{Equation 1})$$

where $f_n(\mathbf{r})$ corresponds to the value of the n^{th} predictor at the spatial coordinates defined by the spatial vector \mathbf{r} , a_n is the coefficient corresponding to each of the predictors, and ε is the unexplained model residual at \mathbf{r} . Note that variable “ x_n ” may be a continuous variable, a categorical variable, or could permit for potential interactions

between two independent variables. It should be noted that the unexplained model residuals (ϵ) were analysed for spatial continuity and clustering using Moran's I index. A statistically significant Moran's I was considered to be a justification towards further developing the LUR model into a UK model. Moran's I index varies between -1 and 1. A Moran's I index of 0 signifies no spatial autocorrelation, whereas values close to -1 and 1 signify spatial dispersion and spatial clustering of model residuals, respectively (Moran 1948). The equation to determine Moran's I index is shown in Equation 2:

$$I = \frac{n}{S_0} \frac{\sum_{i=1}^n \sum_{j=1}^n w_{i,j} (z_i - \bar{z})(z_j - \bar{z})}{\sum_{i=1}^n (z_i - \bar{z})^2} \quad (\text{Equation 2})$$

where n is the number of observations, z_i and z_j correspond to the model residual values at spatial locations i and j, $w_{i,j}$ corresponds to the spatial weight between features i and j, and S_0 corresponds to the sum of all weights. Moran's I index was determined using the "Spatial Autocorrelation" tool under the "Spatial Statistics" toolbox in ArcMap 10.6.2 (ESRI 2018).

2- Universal kriging model

UK models assume that a non-stationary variable, such as groundwater salinity, can be expressed as the sum of a linear empirical model (a trend) along with a stochastic geospatial component that is able to account for spatial correlations. The linear component estimates the expected value of the variable at the sampled spatial locations, rendering the stochastic component ideally intrinsic, with zero expectation, and with a finite variance (Journel and Huijbregts 1978, Kumar 2007). For this study, the statistically significant predictors from the established LUR were used in the UK model to form its linear component (Xu et al. 2019). The geospatial component on the UK model on the other hand is capable of accounting for the spatial correlations in the LUR

model residuals that may be attributed to clustering near major saltwater or freshwater conduits. The overall UK model structure is shown in Equation 3:

$$\log(TDS) [\mathbf{r}] = \sum_{i=1}^n a_n f_n(\mathbf{r}) + \mu(\mathbf{r}) + \varepsilon \quad (\text{Equation 3})$$

where $\mu(\mathbf{r})$ corresponds to the spatially interpolated residual at a spatial location defined by the vector \mathbf{r} , $f_n(\mathbf{r})$ corresponds to the value of the n^{th} predictor at the spatial coordinates defined by \mathbf{r} , a_n is the coefficient corresponding to each of the predictors, and ε is the unexplained white noise. A suitable UK semi-variogram model needs to be selected to model $\mu(\mathbf{r})$. This was based on finding the semi-variogram model that showed the closest fit with the experimental semi-variogram generated from the LUR model residuals. The experimental semi-variogram was constructed using Equation 4 (Matheron 1963):

$$\gamma(h) = \frac{1}{2|N(h)|} \sum_{N(h)} (z_i - z_j)^2 \quad (\text{Equation 4})$$

where $\gamma(h)$ is the experimental semi-variogram value at a lag distance h , $N(h)$ is the set of all pairwise observations separated by h , $|N(h)|$ is the number of distinct pairs in $N(h)$, and z_i and z_j correspond to the observation values in each of the distinct pairs of $N(h)$. Note that since depth was accounted for in the deterministic part of the LUR model, the adopted geo-statistical model was only defined in 2D (longitude and latitude).

The minimization of the UK estimation variance results in a set of linear equations that are simultaneously solved to estimate the coefficients of the linear model (a_n) and the coefficients of the geo-spatial model (μ_r) concurrently (Ver Hoef and Cressie 1993). The geospatial model coefficients include the nugget, sill, and range of the semi-variogram model. The nugget, ideally zero, represents the variance of the response variable as separation distances approach zero. The sill represents the semi-

variogram limiting value, after which, no spatial correlations exist. Meanwhile, the range represents the distance in meters at which the sill is reached (Armstrong 1998). UK model fitting was done using the “gstat” package (Pebesma 2004) in the R software (R Core Team 2018). Three different semi-variogram models were considered to estimate the correlation structure, namely the “Gaussian”, “Exponential”, and “Spherical”. The best model was selected based on several leave-one-out cross-validation (LOOCV) prediction statistics that included the NSE, the Root Mean Square Error (RMSE), and the residual standard deviation (RSD).

3- Model comparison and SWI mapping

For each of the two models, predictive salinity surfaces were generated for the study area at well depths of 50 m, 100 m, and 150 m. These three depths were selected to cover the range of depths in the sampled wells. Mean salinity predictions were generated on a 10 m × 10 m raster grid that covered the geographical extent of the study area. This was achieved using both the “sf” package (Pebesma 2018) in R (R Core Team 2018) as well as the “Spatial Analysis Toolbox” in ArcMap 10.6.2 (ESRI 2018). Note that since both the LUR and UK models can potentially predict concentrations with salinities exceeding the levels of the Mediterranean Sea (TDS = 35,000 ppm), any prediction above 35,000 ppm was truncated and replaced with a value of 35,000 ppm (Goovaerts 1997). The performance of the UK model versus that of the LUR was evaluated by calculating the differences in the predicted salinity levels (Equation 5), comparing prediction uncertainties (variances) over space, as well as by assessing a set of LOOCV statistics (Table 2). The LOOCV statistics that were used for model comparison included: the NSE, PBIAS, RMSE, the root mean square standardized error

(RMS-S), and the ratio of RMSE to the standard deviation of observations (RSR; Table 2).

$$Diff_{i,j} = \mu_{i,j}^{LUR} - \mu_{i,j}^{UK} \quad (\text{Equation 5})$$

where $\mu_{i,j}^{LUR}$ is the mean predicted salinity value from the LUR model at location i, j for a specific depth and $\mu_{i,j}^{UK}$ is the mean predicted salinity value from the UK model at location i, j for a specific depth.

Table 2: Model performance statistics

Performance statistics	Formula
Nash-Sutcliffe Efficiency (NSE)	$NSE = 1 - \frac{\sum(Y_i^{obs} - Y_i^{sim})^2}{\sum(Y_i^{obs} - \gamma^{mean})^2}$
Percent bias (PBIAS)	$PBIAS = \frac{\sum(Y_i^{obs} - Y_i^{sim}) * 100}{\sum Y_i^{obs}}$
Root Mean Squared Error (RMSE)	$RMSE = \sqrt{\frac{\sum(Y_i^{obs} - Y_i^{pred})^2}{n}}$
Root Mean Square Standardized Error (RMS-S)	$RMS - S = \frac{RMSE}{STDEV_{pred}} = \sqrt{\frac{\sum(Y_i^{obs} - Y_i^{sim})^2}{n * \hat{\sigma}^2}}$
Ratio of RMSE to standard deviation of observations (RSR)	$RSR = \frac{RMSE}{STDEV_{obs}} = \frac{\sqrt{\sum(Y_i^{obs} - Y_i^{sim})^2}}{\sqrt{\sum(Y_i^{obs} - \gamma^{mean})^2}}$

CHAPTER III

RESULTS AND DISCUSSION

A- Saltwater intrusion in the Beirut Aquifer

Salinity levels recorded during the 2018-2019 sampling campaign showed a large spatial variability across the study area. Groundwater TDS levels ranged from as low as 250 ppm up to 35,000 pm, while chloride levels ranged from as low as 15 ppm up to 28,000 ppm (Figure 4). As expected, chlorides were highly correlated to measured TDS levels (Pearson's correlation coefficient of 0.99). Salinity levels were found to vary significantly between the different administrative regions of the city (Figure 5). Wells located in the geologically unprotected zone that experiences chronic water shortages (Figure 3) showed significantly higher levels of salinity as compared to wells located in the geologically protected zone of the city that has ample water supply (Figure 6). The quality of the groundwater in the latter was exclusively fresh, while the quality of the former ranged largely from brackish to saline. Another clear spatial pattern of the variability in salinity levels was the drop in the salinity moving away from the coastline (Figure 7), with levels beyond 2 km of the coastline stabilizing at 500 ppm. Note that some sections of the Mazraa administrative region, which experiences chronic water shortages and is unprotected geologically from SWI, had salinity levels similar in magnitude to those observed in the geologically protected zones of the city that received an ample supply of freshwater, largely because it is the farthest inland region of Beirut.

In addition to the observed large-scale spatial patterns of salinity, small-scale heterogeneities were recorded within several regions, particularly in the areas of Moussaytbeh, Ras Beirut, Ain-Mreisseh, Mina el-Hosn, and Zkak el Blatt. This small-

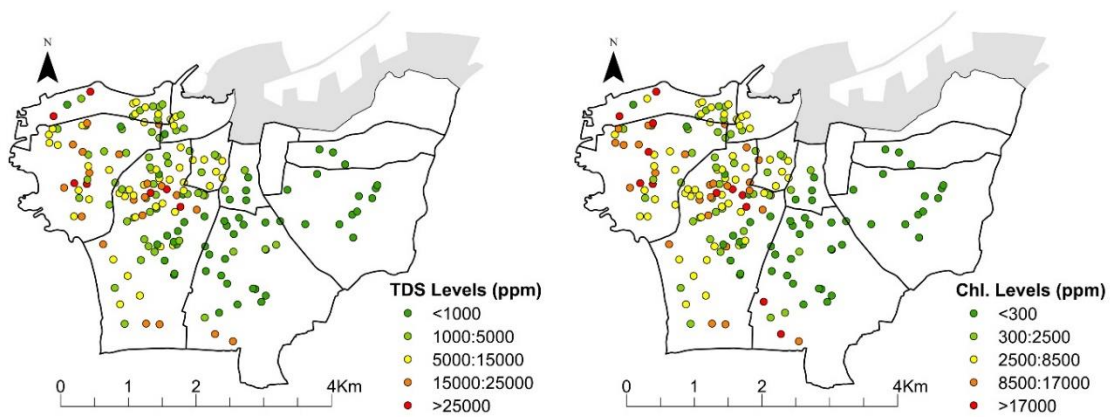


Figure 4: Measure TDS (a) and chloride (b) levels during the sampling campaign of 2018-2019

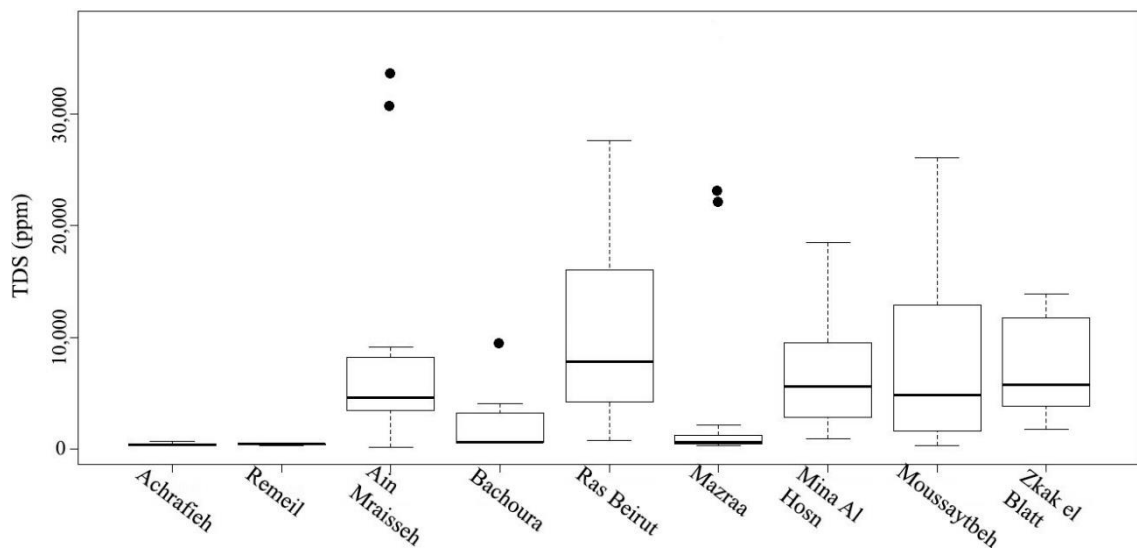


Figure 5: TDS levels across the different administrative zones of Beirut (no wells were sampled in Saifi and Medawar)

scale variability was partly due to the observed differences in well depths. The range of well depths was found to vary the most in these areas, particularly in the regions in close proximity to the sea. As expected, deeper wells in a given area tended to be at a higher risk of salinization (Herzberg 1901). In Beirut, we found that the salinity levels in the sampled wells tended to increase linearly with well depth (Pearsons's correlation coefficient of 0.62) up to 700 m away from the coastline. The correlations weakened at

larger distances, potentially because the saltwater freshwater interphase became too deep to affect the tapped wells (Herzberg 1901).

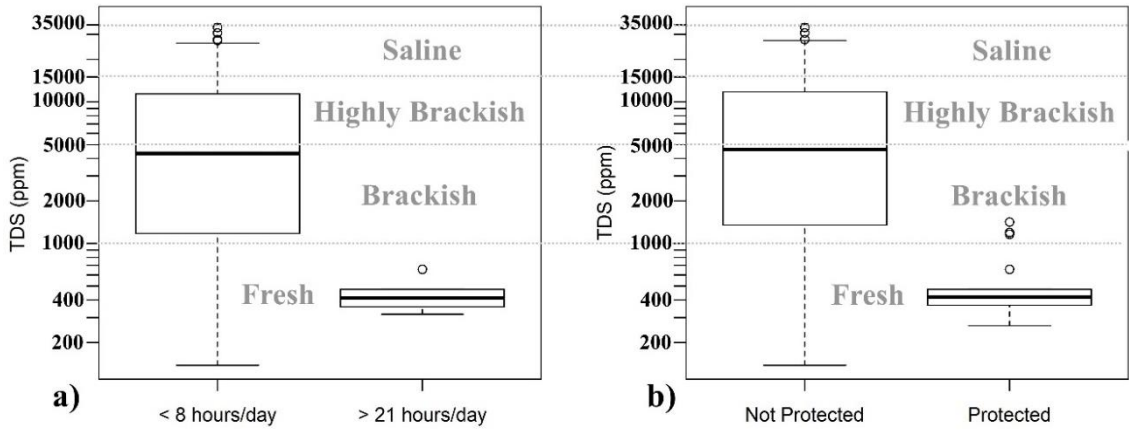


Figure 6: Variation of observed TDS as a function of a) frequency of fresh water supply and b) the presence of geological protection

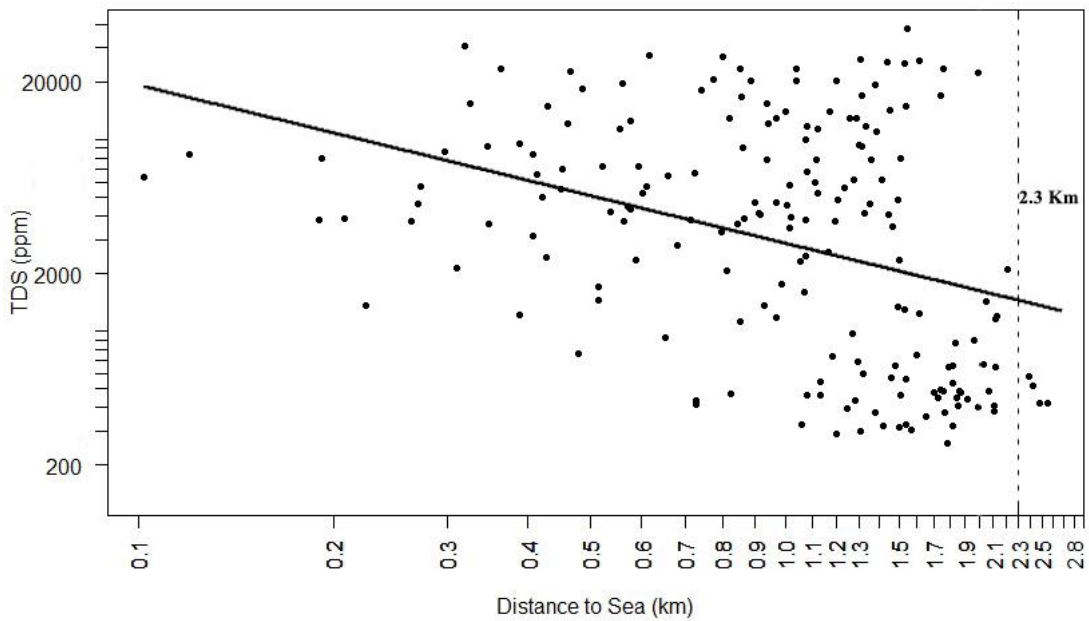


Figure 7: Variation of measured TDS levels as a function of distance to coastline

In an effort to quantify the temporal changes in salinity levels in the study area, the measured salinity levels from the 2018-2019 dry season were compared to those measured previously during the same season back in 2013 (Alameddine et al. 2018, Momejian et al. 2019b). Paired t-tests were conducted on data collected from 44 wells that were sampled during both campaigns. Both the median TDS and chloride levels were found to have significantly increased over the past 5 years, from around 3,600 ppm to more than of 5,100 ppm for TDS and from 1,900 ppm to 3,550 ppm for chlorides (p-values of 4×10^{-3} and 9×10^{-5} respectively), indicating that SWI in these 44 wells has accelerated at an alarming rate.

B- SWI model predictions and performance

The LUR model developed for predicting TDS levels in the study area was able to explain 60% of the observed variability. The final model had five significant predictors (Table 3) that included the distance separating the well from the coastline, well depth, elevation, the presence of geological protection, and the number of buildings with water desalination units within a buffer zone of 200 m. The model predicted that for every 10% increase in the separation distance between a well and the coastline, the salinity was expected to drop by around 10% on average; meanwhile increasing the depth of a well by 10 % resulted in a 9% increase in its salinity level. Wells in the zone that were geologically protected against SWI had salinities that were on average 75% lower than similar wells in the unprotected zone of the city. Additionally, the model predicted that for every one meter increase in elevation, the average TDS levels were predicted to drop by around 3%. Lastly, for every additional building within a 200 m buffer zone from a well that is fitted with a desalination unit, the model predicted a 14%

increase in the geometric mean of its TDS level. The influence of the desalination units and elevation was found to be localized to a few areas; yet their relative influence increased with depth. It should be noted that several of the considered predictors were not selected in the final model due to high multi-collinearity between the predictors. For example, the large overlap between the geologically protected zone and the regions of the city that received more than 21 hours/day of freshwater supply did not allow for including the two categorical variables in the same model. Interestingly, the categorical variable describing the period during which intensive urbanisation happened in the city turned out to be statistically not significant with regards to predicting the salinity levels in the city. We believe that this might be attributed to two main reasons. The first reason is the high penetration of groundwater wells in the newly developed part of the city as compared to the older sections of the city. As such, it appears that while new section of the city had a shorter period of groundwater over-pumping, the rate appears to be much higher than in other parts of the city. The second reason could be attributed to the presence of the dense suburb of Beirut just south of the newly developed part of the city. That suburb faces chronic water shortages even more severe than the western section of Beirut City and as such it relies heavily on groundwater resources.

Overall, the model predicted that freshwater was expected to occur in 43 % of the study area at a well depth of 50 m (Figure 8). This percentage decreased with depth and reached around 19% at a depth of 150 m. Meanwhile, the areas that were expected to tap into saline water increased from less than 11% at a depth of 50 m to more than 23 % at a depth of 150 m. Overall and across all depths, the most common salinity level to expect was brackish water (Figure 8). Moreover, the LUR prediction maps captured the

two most important SWI dynamics that include having the salinity levels decrease moving away from the coastline, while at the same time increasing with depth (Figure 9). The model predictions also clearly delineated the separation between the geologically protected region of the study area from that which lacked it.

Table 3: Developed LUR model for predicting log(TDS)

Predictor	Model coefficient (± 1 sd)	p-value
Intercept	12.53 (± 1.57)	5.38×10^{-11}
Geologically Protected Zones (categorical)	-1.33 (± 0.41)	1.87×10^{-3}
Log of distance to sea (m)	-1.15 (± 0.32)	7.63×10^{-4}
Log of well depth (m)	0.88 (± 0.30)	4.95×10^{-3}
Number of buildings with desalination units within a 200 m radius	0.13 (± 0.06)	0.04
Elevation (m)	-0.03 (± 0.016)	0.09
$R^2 = 0.6$; Adjusted $R^2 = 0.58$; NSE=0.54; RMSE = 0.928; RSD= 0.936, PBIAS=0.13%		

In terms of model performance, the obtained LUR model was highly significant (F-statistic = 17.48; p-value = 1.40×10^{-10}) and had a relatively high adjusted R^2 (58 %). The model was also found to be robust given that its LOOCV NSE was 54%. In addition, the model had a RMSE and RSD of 0.928 and 0.936 respectively and a negligible PBIAS of 0.13%. Exploring the LUR model residuals for spatial patterns, we found that they had a highly significant positive Moran's I index (value=0.34, p-value= 3.5×10^{-4}). This indicates the occurrence of geospatial clustering that was not resolved by the LUR model.

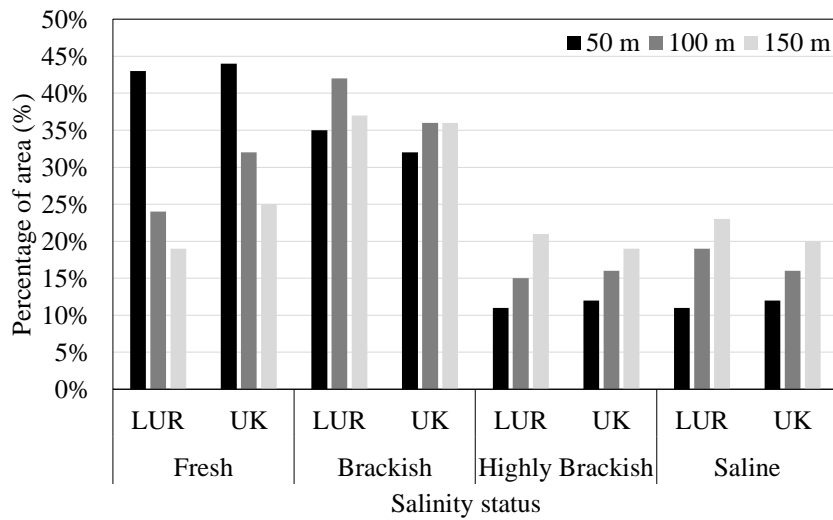


Figure 8: Predicted salinity level status of groundwater as a function of well depth for the Land Use Regression (LUR) model and the Universal Kriging (UK) model

The fitted UK model was able to account for the statistically significant geospatial correlations that persisted after de-trending. The model's assumption of spatial isotropy was confirmed by the lack of directional variations in the constructed 2D experimental variogram map of the LUR model residuals. Note that this finding is typical, as the regression part of the UK model is often able to account to a large extent for the spatial anisotropies in the collected data (Caballero et al. 2013, Deviren et al. 2013, Somayasa et al. 2019, Xu et al. 2019). Three different isotropic correlation structures were explored to account for the geospatial correlations in the data, namely the exponential, Gaussian, and spherical semi-variogram models. The adoption of an exponential semi-variogram proved to be the most optimal, as it had the highest LOOCV NSE, the lowest LOOCV RMSE, and the smallest LOOCV residual standard deviation (Table 4). The exponential semi-variogram model had a range of 248 m, indicating that the spatial autocorrelation of salinity in the study area was restricted to relatively short distances.

Table 4: Leave-one-out cross-validation (LOOCV) based statistics for three semi-variogram UK models

Model	LOOCV NSE	LOOCV RMSE	LOOCV RSD
LUR	0.54	0.928	0.94
Spherical	0.69	0.77	0.77
Gaussian	0.69	0.76	0.77
Exponential	0.71	0.74	0.74

Similar to the LUR, the UK model was able to capture the dynamics of the salinity level changes as a function of distance to sea and well depth (Figure 9). All LUR predictors remained statistically significant in the UK model and their coefficients remained largely unchanged. As such, the predictions of the UK and LUR models were highly correlated (Pearson's correlation = 0.93) and showed relatively good agreement with regards to their predictions in the study area. Nevertheless, the two models diverged in their predictions in a few areas, especially in the geologically unprotected zones. In those regions, differences in model predictions reached as high as 20,000 ppm (Figure 9). These large discrepancies were primarily due to the ability of the UK model to extract and account for the spatial information found in the correlated LUR model residuals. This allowed the UK model to more faithfully account for potential fine-scale (≤ 248 m) geological irregularities in the Beirut karst aquifer, such as the presence of freshwater/saltwater conduits that tend to have high hydraulic conductivities. For example, in some areas along the north-western sections of the study area (Zone A in Figure 9), the UK model predicted significantly lower salinity levels as compared to the

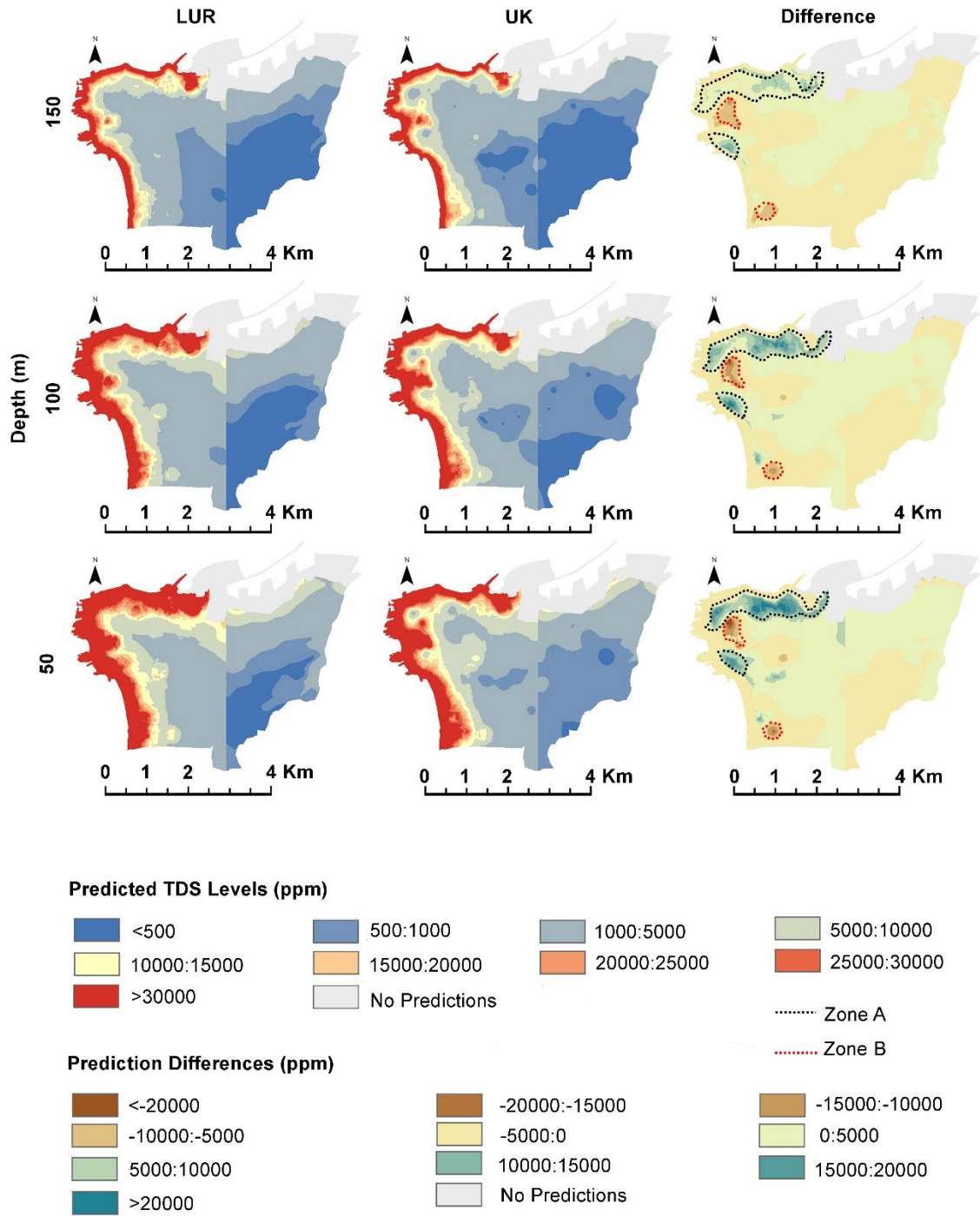


Figure 9: Predicted salinity levels as a function of depth. The first column shows the LUR-based predictions; the second column plots the UK-based estimates; the third column shows the difference in predictions between the two models (LUR - UK)

LUR model, pointing to the possibility of a freshwater conduit in that region or to elevated recharge. Meanwhile, the UK model predicted that the south-western corner of

the study area as well as sections in the north-western parts of the city (Zone B in Figure 9) had higher salinity levels as compared to the LUR and as such the location of the saltwater wedge was extended deeper inland.

In an effort to assess the predicted variability in the salinity levels over depth across the study area, two salinity-level cross-sections were produced by stacking predicted salinity maps generated at a 1 m depth interval. The first cross section (AA') was selected so as to cut through the geologically unprotected region of the city, while the second (BB') extended along the geologically protected zone. Examining the AA' cross-section, we see that the both models predicted that the saltwater wedge extended to around 1.13 Km inland at a depth of 150 m (Figure 10). Yet, the UK-based cross-section clearly showed evidence of up-coning occurring at a distance of around 2 Km from the coastline. Interestingly, that area was also identified by Safi (2019) to be experiencing upconing. No evidence of upconing was apparent in the LUR based cross-section. Along section BB', the wedge in both models was found to be limited to the area in the immediate vicinity to the coastline, highlighting the importance of both the geological protection and the ample water supply provided to that region in impeding SWI.

Regarding the performance of the two models, the UK model outperformed the LUR model across most model performance metrics. The UK's NSE was 32% higher, its RMSE was 20% lower, and its residual standard deviation was 20% smaller (Table 4). It also had a better cross validation robustness as seen in the generated LOOCV

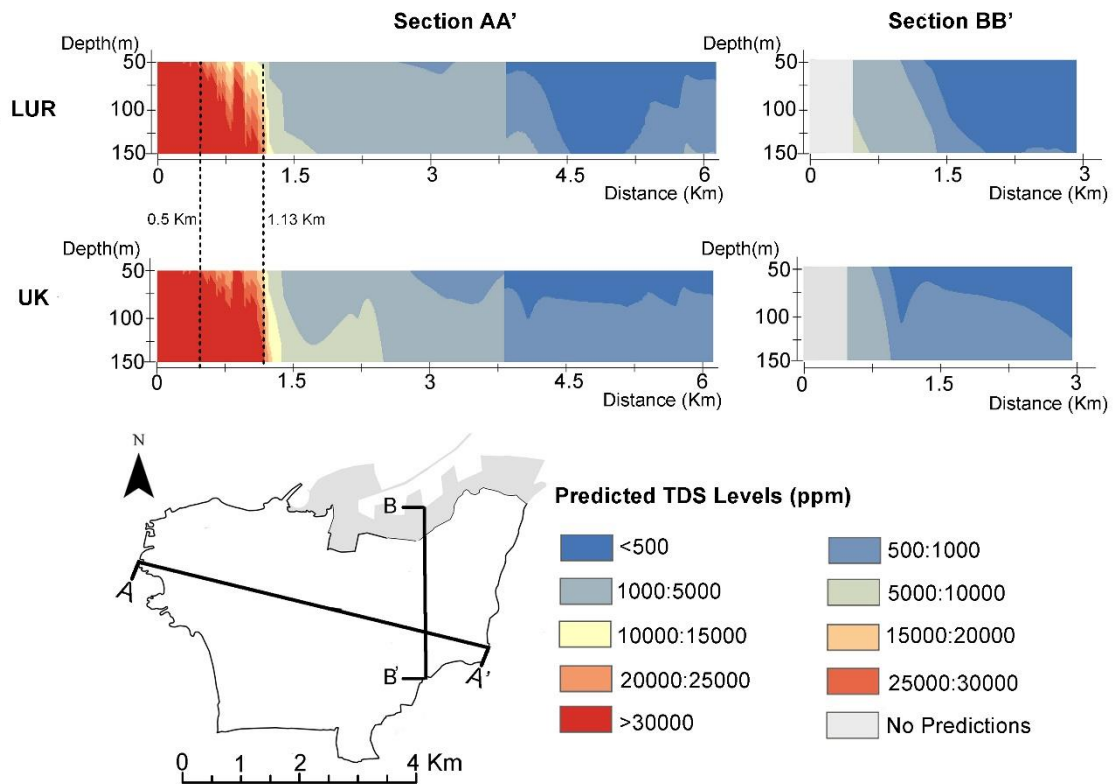


Figure 10: Predicted TDS levels along two cross-sections at a depth of 150 m. The x-axis represents the distance (Km) and the y-axis represents the depth (m)

predicted versus observed plots, whereby the UK predictions were more correlated with the observed values (R^2 for UK 0.70 versus 0.53 for LUR) and showed a lower bias (slope for UK is 0.73 versus 0.59 for LUR) (Figure 11). Moreover, the UK model was able to significantly reduce the prediction uncertainties across the prediction spatial domain (Figure 12). On average, the reduction in the prediction variance in log(TDS)-scale across the entire study domain was close to 20%, with some locations experiencing a reduction in prediction variance in excess of 95%. As expected, zones that had a high density of sampled wells, such as in the Moussaytbeh and Ras-Beirut areas, witnessed the largest reduction in prediction variance (Figure 12), whereas the area of Medawar that did not include any sampling well had the highest levels of prediction variance in

both models. Note that the reductions in prediction variance were consistent across the three assessed depths (50 m, 100 m, and 150 m).

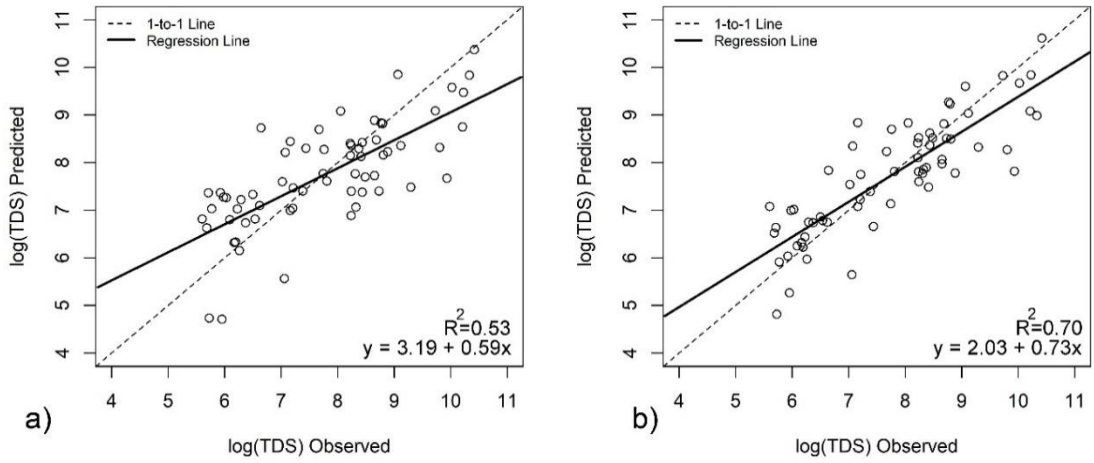


Figure 11: Predicted versus observed log(TDS) levels for a) the LUR model and b) the UK model. The plot shows the regression line between predicted and observed along with the 1:1 line

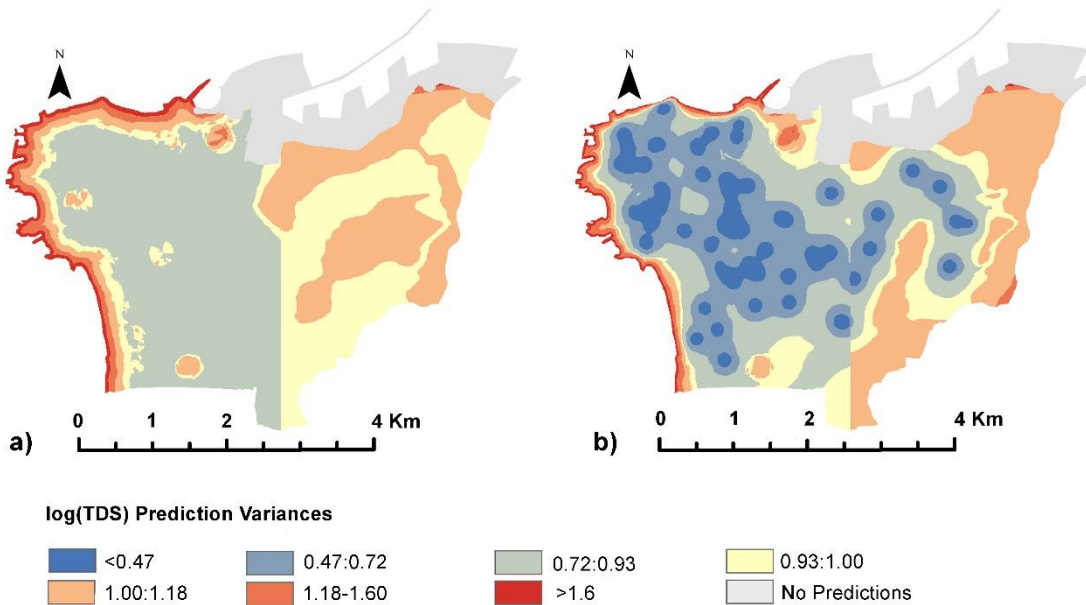


Figure 12: Log(TDS) prediction variances at a depth of 100 m for a) LUR predictions and b) UK predictions

Overall, both of the developed LUR and the UK model showed significantly better performances as compared to other SWI model developed for the area. For example, the kriging model that was generated for the same study area by Momejian et al. (2019b) was reported to have a percent bias in excess of 75%, a RMS-S of 1.69, and a RSR of 0.9. The percent bias of both the LUR and UK models was less than 0.5% and their RSRs were significantly lower (0.7 and 0.5 respectively). Additionally, the RMS-S of the LUR model was half that of the kriging model, while the UK's was less than one third of the latter. Moreover, the predictive skills of both our LUR and UK models were substantially higher than those reported by (Momejian et al. 2019a) for the DRASTIC and EPIK model they developed for the same study area, where their prediction correlations with 5 predefined TDS-based water quality groups was found to be less than 30 %.

CHAPTER IV

CONCLUSIONS

The model results showed the extent of the SWI problem in Beirut, whereby around a third of the groundwater in the city at a depth of 100 m was predicted to be highly brackish to saline. The model also showed substantial spatial differences in the water quality between the eastern sections of the city as compared to the western neighbourhoods. These large spatial patterns were largely attributed to marked differences in geology (aquifer and stratigraphy) and water delivery. The saltwater wedge in the SWI affected western neighbourhoods was found to extend 1.13 km inland. These findings highlight the significant degradation of groundwater quality in Beirut, as a result of chronic water shortages and poor groundwater management. It is estimated that there were around 10,000 licensed private wells in Lebanon and more than 40,000 illegal wells back in 2003. That number is expected to have grown considerably since then and will most probably continue to increase as the city continues to grow and water deficits intensify (World Bank 2003). Moreover, the increased market penetration of the poorly designed and low-efficiency small-scale RO desalination units in the city is expected to further exacerbate the problem. Without an urgent and sustainable city-wide plan that aims to bridge the gap between supply and demand, while also introducing demand management interventions, such as restructuring the water tariff system and introducing smart metering, larger sections of the aquifer will start feeling the impacts of SWI as the wedge continues to move inland fuelled by over pumping and dwindling permeable areas needed for recharge.

This study is the first of its kind to apply a UK approach to quantify and map SWI along a coastal aquifer. The UK model outperformed the LUR model and previous kriging and groundwater vulnerability models developed for the area. The superior performance of the developed model is attributed to its ability to account for important socio-economic, land-use/land-cover, and geological/geographical drivers of SWI, while at the same time harnessing the significant spatial autocorrelations in the sampled data. Distance to sea, well depth, the presence of a protective geological layer against SWI, elevation, and the number of buildings with water desalination units all proved to be important determinants of salinity levels in the study area. Alone they were able to explain around 60% of the variability observed in the data. Moreover, accounting for the spatial correlation data further improved the model. The NSE of the UK model reached 71% as compared to 54% for the LUC model. The UK model showed that significant spatial-autocorrelations in salinity levels existed up to a range of 248 m. Capturing these spatial dependencies is particularly important in an urban karst environment that is known to have high hydro-geological heterogeneity, numerous faults and conduits, and varying levels of pumping over space. As a result, the UK model was able to identify inland areas in the city that are experiencing upconing and the coastal sections of the city that had more pronounced saltwater wedges. At the same time, the model highlighted the sections of the city that appear to be benefiting from the presence of freshwater conduits or from elevated recharge. Moreover, the model was able to identify locations in the city with high uncertainties regarding their salinity levels. As such, future monitoring programs should make an effort to sample more wells from these poorly characterized regions.

Finally, the results of this study provide a promising modelling and mapping approach that can be implemented to map SWI in poorly monitored urban coastal aquifers and to better understand their vulnerabilities to anthropogenic stressors. Areas where the UK model has predicted significantly higher or lower salinity levels as compared to the LUR are expected to have significant hydro-geological irregularities, including elevated local recharge, prevalence of major saltwater/freshwater conduits, and a high density of fractures. These regions are in need of a detailed hydro-geological investigation in order to further characterize their subsurface.

The proposed method is expected to outperform most mathematical models in mapping SWI in study areas similar to Beirut that are karstic, highly urbanized, and suffer from the scarcity of hydro-geological data. Thus, the potential of this work to help generate a comprehensive SWI map for the poorly monitored groundwater aquifers all along the Eastern Mediterranean coastline is tremendous.

REFERENCES

- Ahmadi, S.H. and Sedghamiz, A. (2006) Geostatistical analysis of spatial and temporal variations of groundwater level. *Environmental monitoring and assessment* 129(1-3), 277-294.
- Akaike, H. (1974) A new look at the statistical model identification. *IEEE Transactions on Automatic Control* 19(6), 716-723.
- Akbarpour, S. and Niksokhan, M.H. (2018) Investigating effects of climate change, urbanization, and sea level changes on groundwater resources in a coastal aquifer: an integrated assessment. *Environmental Monitoring and Assessment* 190(10), 579.
- Alameddine, I., Tarhini, R. and El-Fadel, M. (2018) Household economic burden from seawater intrusion in coastal urban areas. *Water International* 43(2), 217-236.
- Allen, D., Abbey, D., Mackie, D., Luzitano, R. and Cleary, M. (2002) Investigation of potential saltwater intrusion pathways in a fractured aquifer using an integrated geophysical, geological and geochemical approach. *Journal of Environmental & Engineering Geophysics* 7(1), 19-36.
- Armstrong, M. (1998) *Basic Linear Geostatistics*, Springer Science & Business Media, Berlin, Heidelberg
- Barlow, P.M. and Reichard, E.G. (2010) Saltwater intrusion in coastal regions of North America. *Hydrogeology Journal* 18(1), 247-260.
- Beebe, C.R., Ferguson, G., Gleeson, T., Morgan, L.K. and Werner, A.D. (2016) Application of an analytical solution as a screening tool for sea water intrusion. *Groundwater* 54(5), 709-718.
- Beirut Urban Lab (2020) Beirut Building Database, American University of Beirut, Beirut, Lebanon.
- Bhattachan, A., Emanuel, R.E., Ardon, M., Bernhardt, E.S., Anderson, S.M., Stillwagon, M.G., . . . Wright, J.P. (2018) Evaluating the effects of land-use change and future climate change on vulnerability of coastal landscapes to saltwater intrusion. *Elem Sci Anth* 6(1), 62.
- Bou-Zeid, E. and El-Fadel, M. (2002) Climate change and water resources in Lebanon and the Middle East. *Journal of Water Resources Planning and Management* 128(5), 343-355.

- Bruington, A.E. (1972) Saltwater intrusion into aquifers. *JAWRA Journal of the American Water Resources Association* 8(1), 150-160.
- Caballero, W., Giraldo, R. and Mateu, J. (2013) A universal kriging approach for spatial functional data. *Stochastic Environmental Research and Risk Assessment* 27(7), 1553-1563.
- CAS (2009) Population characteristics in 2009 - final report, The Central Administration of Statistics, Beirut, Lebanon.
- Chang, S.W., Clement, T.P., Simpson, M.J. and Lee, K. (2011) Does sea-level rise have an impact on saltwater intrusion? *Advances in water resources* 34(10), 1283-1291.
- Cimino, A., Cosentino, C., Oieni, A. and Tranchina, L. (2008) A geophysical and geochemical approach for seawater intrusion assessment in the Acquedolci coastal aquifer (Northern Sicily). *Environmental Geology* 55(7), 1473-1482.
- CNRS (2010) Lebanese Land Use and Land Cover (LULC) Map, National Center For Remote Sensing, Beirut, Lebanon.
- Dai, D., Sun, M., Xu, X. and Lei, K. (2019) Assessment of the water resource carrying capacity based on the ecological footprint: a case study in Zhangjiakou City, North China. *Environmental Science and Pollution Research International* 26(11), 11000-11011.
- de Hoogh, K., Wang, M., Adam, M., Badaloni, C., Beelen, R., Birk, M., . . . Hoek, G. (2013) Development of land use regression models for particle composition in twenty study areas in Europe. *Environmental Science & Technology* 47(11), 5778-5786.
- Deng, Y., Young, C., Fu, X., Song, J. and Peng, Z.-R. (2017) The integrated impacts of human activities and rising sea level on the saltwater intrusion in the east coast of the Yucatan Peninsula, Mexico. *Natural Hazards* 85(2), 1063-1088.
- Dentoni, M., Deidda, R., Paniconi, C., Qahman, K. and Lecca, G. (2015) A simulation/optimization study to assess seawater intrusion management strategies for the Gaza Strip coastal aquifer (Palestine). *Hydrogeology Journal* 23(2), 249-264.
- Deviren, M.N., Arikan, F. and Arikan, O. (2013) Automatic regional mapping of total electron content using a GPS sensor network and isotropic universal kriging, pp. 1664-1669, IEEE.
- Dubertret, L. (1955) *Cartes Géologiques du Liban 1:50000: Feuille de Beirut*, Délégation Générale de France au Levant, Section Géologique, Beirut, Lebanon.

- Dubois, C., Goderniaux, P., Deceuster, J., Poulain, A. and Kaufmann, O. (2019) Hydrogeological characterization and modelling of weathered karst aquifers. Applicability to dewatering operations in limestone quarries. *Environmental Earth Sciences* 78(3), 1-18.
- EBML (2019) Water supply for Beirut City: 2019, Beirut, Lebanon.
- Eeftens, M., Beelen, R., de Hoogh, K., Bellander, T., Cesaroni, G., Cirach, M., . . . Hoek, G. (2012) Development of land use regression models for PM_{2.5}, PM_{2.5} absorbance, PM₁₀ and PM coarse in 20 European study areas: results of the ESCAPE project. *Environmental Science & Technology* 46(20), 11195-11205.
- El-Fadel, M., Maroun, R., Semerjian, L. and Harajli, H. (2003) A health-based socio-economic assessment of drinking water quality: the case of Lebanon. *Management of Environmental Quality* 14(3), 353-368.
- El-Fadel, M., Rachid, G., Alameddine, I. and Abu Najm, M. (2014) Saltwater intrusion in karst aquifers along the Eastern Mediterranean, SWIM, Husum, Germany.
- Elewa, H.H., Shohaib, R.E., Qaddah, A.A. and Nousir, A.M. (2013) Determining groundwater protection zones for the quaternary aquifer of northeastern Nile delta using GIS-based vulnerability mapping. *Environmental Earth Sciences* 68(2), 313-331.
- ESRI (2018) ArcGIS Desktop: Release 10.6, Redlands, CA.
- Famiglietti, J.S. (2014) The global groundwater crisis. *Nature Climate Change* 4(11), 945-948.
- FAO (1997) Seawater intrusion in coastal aquifers: Guidelines for study, monitoring and control, Food & Agriculture Organization of the United Nations, Rome, Italy
- Flores, L., Bailey, R.T. and Kraeger-Rovey, C. (2020) Analyzing the effects of groundwater pumping on an urban stream aquifer system. *JAWRA Journal of the American Water Resources Association* 56(2), 310-322.
- Foulon, É. and Rousseau, A.N. (2019) Surface water quantity for drinking water during low flows - sensitivity assessment solely from climate data. *Water Resources Management* 33(1), 369-385.
- Giambastiani, B.M.S., Antonellini, M., Oude Essink, G.H.P. and Stuurman, R.J. (2007) Saltwater intrusion in the unconfined coastal aquifer of Ravenna (Italy): A numerical model. *Journal of Hydrology* 340(1), 91-104.
- Goovaerts, P. (1997) Geostatistics for natural resources evaluation, Oxford University Press on Demand, New York, NY

Gorelick, S.M. and Zheng, C. (2015) Global change and the groundwater management challenge. *Water Resources Research* 51(5), 3031-3051.

Gorgij, A.D. and Moghaddam, A.A. (2016) Vulnerability assessment of saltwater intrusion using simplified GAPDIT method: a case study of Azarshahr Plain aquifer, east Azerbaijan, Iran. *Arabian Journal of Geosciences* 9(2), 106.

Green, T.R. (2016) *Integrated Groundwater Management: Concepts, Approaches and Challenges*. Jakeman, A.J., Barreteau, O., Hunt, R.J., Rinaudo, J.-D. and Ross, A. (eds), pp. 97-141, Springer Open.

Gundogdu, K.S. and Guney, I. (2007) Spatial analyses of groundwater levels using universal kriging. *Journal of earth system science* 116(1), 49-55.

Heather, C., Newsha, A., Mai-Lan, H. and Veena, S. (2014) *The World's Water - The Biennial Report on Freshwater Resources*. Gleick, P. (ed), pp. 1-3, Island Press.

Herzberg, A. (1901) Die wasserversorgung einiger Nordseebader. *Journal Gasbeleucht und Wasserversorg* 44, 842-844.

Hoek, G., Beelen, R., Kos, G., Dijkema, M., Zee, S.C.v.d., Fischer, P.H. and Brunekreef, B. (2011) Land use regression model for ultrafine particles in Amsterdam. *Environmental Science & Technology* 45(2), 622-628.

Huang, P.-S. and Chiu, Y.-C. (2018) A simulation-optimization model for seawater intrusion management at Pingtung coastal area, Taiwan. *Water* 10(3), 251-279.

Hussien, W.e.A., Memon, F.A. and Savic, D.A. (2016) Assessing and modelling the influence of household characteristics on per capita water consumption. *Water Resources Management* 30(9), 2931-2955.

Imad, E. (2003) Prevention of seawater intrusion by the artificial recharge of groundwater on the Lebanese coast, The Mediterranean Agronomic Institute of Bari, Valenzano, Italy.

ISO (1989) *Water quality - determination of chloride - silver nitrate titration with chromate indicator (Mohr's method)*.

Jakeman, A.J., Barreteau, O., Hunt, R.J., Rinaudo, J.-D., Ross, A., Arshad, M. and Hamilton, S. (2016) *Integrated Groundwater Management: Concepts, Approaches, and Challenges*. Jakeman, A.J., Barreteau, O., Hunt, R.J., Rinaudo, J.-D. and Ross, A. (eds), pp. 3-20, Springer Open.

Journel, A.G. and Huijbregts, C.J. (1978) *Mining Geostatistics*, Academic Press, London, UK

- Kerrou, J., Renard, P., Cornaton, F. and Perrochet, P. (2013) Stochastic forecasts of seawater intrusion towards sustainable groundwater management: application to the Korba aquifer (Tunisia). *Hydrogeology Journal* 21(2), 425-440.
- Kerrou, J., Renard, P., Lecca, G. and Tarhouni, J. (2010a) Grid-enabled Monte Carlo analysis of the impacts of uncertain discharge rates on seawater intrusion in the Korba aquifer (Tunisia). *Hydrological Sciences Journal* 55(8), 1325-1336.
- Kerrou, J., Renard, P. and Tarhouni, J. (2010b) Status of the Korba groundwater resources (Tunisia): observations and three-dimensional modelling of seawater intrusion. *Hydrogeology Journal* 18(5), 1173-1190.
- Klassen, J. and Allen, D.M. (2017) Assessing the risk of saltwater intrusion in coastal aquifers. *Journal of Hydrology* 551, 730-745.
- Kourgialas, N.N., Dokou, Z., Karatzas, G.P., Panagopoulos, G., Soupios, P., Vafidis, A., . . . Schafmeister, M. (2016) Saltwater intrusion in an irrigated agricultural area: combining density-dependent modeling and geophysical methods. *Environmental Earth Sciences* 75(1), 1-13.
- Kumar, V. (2007) Optimal contour mapping of groundwater levels using universal kriging-a case study. *Hydrological Sciences Journal* 52(5), 1038-1050.
- Kura, N.U., Ramli, M.F., Ibrahim, S., Sulaiman, W.N.A., Zaudi, M.A. and Aris, A.Z. (2014) A preliminary appraisal of the effect of pumping on seawater intrusion and upconing in a small tropical island using 2D resistivity technique. *The Scientific World Journal* 2014.
- Lal, A. and Datta, B. (2019) Optimal groundwater-use strategy for saltwater intrusion management in a pacific island country. *Journal of Water Resources Planning and Management* 145(9).
- Langevin, C.D. and Zygnerski, M. (2013) Effect of sea-level rise on salt water intrusion near a coastal well field in southeastern Florida. *Groundwater* 51(5), 781-803.
- Lebanese Army (1950) Aerial imagery of Beirut City. Directorate of Geographic Affairs (ed), Ministry of Defense, Beirut, Lebanon.
- Lobo-Ferreira, J.P., Chachadi, A.G., Diamantino, C. and Henriques, M.J. (2005) Assessing aquifer vulnerability to sea-water intrusion using GALDIT method: Part 1 – application to the Portuguese aquifer of Monte Gordo, Guimaraes, Portugal.
- Ma, X., Longley, I., Gao, J., Kachhara, A. and Salmond, J. (2019) A site-optimised multi-scale GIS based land use regression model for simulating local scale patterns in air pollution. *Science of the Total Environment* 685, 134-149.

- Mahesha, A., Vyshali, A.M., Lathashri, U.A. and Ramesh, H. (2012) Parameter estimation and vulnerability assessment of coastal unconfined aquifer to saltwater intrusion. *Journal of Hydrologic Engineering* 17(8), 933-943.
- Mancuso, M., Santucci, L. and Carol, E. (2020) Effects of intensive aquifers exploitation on groundwater salinity in coastal wetlands. *Hydrological Processes* 34(11), 2313-2323.
- Mantoglou, A. (2003) Pumping management of coastal aquifers using analytical models of saltwater intrusion. *Water Resources Research* 39(12), 1335-1348.
- Masterson, J.P. and Garabedian, S.P. (2007) Effects of sea-level rise on ground water flow in a coastal aquifer system. *Groundwater* 45(2), 209-217.
- Matheron, G. (1963) Principles of geostatistics. *Economic Geology* 58(8), 1246-1266.
- Mehdizadeh, S.S., Vafaie, F. and Abolghasemi, H. (2015) Assessment of sharp-interface approach for saltwater intrusion prediction in an unconfined coastal aquifer exposed to pumping. *Environmental Earth Sciences* 73(12), 8345-8355.
- Mekonnen, M. and Hoekstra, A.Y. (2016) Four billion people facing severe water scarcity. *Science Advances* 2(2).
- Metni, M., El-Fadel, M., Sadek, S., Kayal, R. and El-Khoury, D. (2004) Groundwater resources in Lebanon: a vulnerability assessment. *International Journal of Water Resources Development* 20(4), 475-492.
- Meyer, R., Engesgaard, P. and Sonnenborg, T.O. (2019) Origin and dynamics of saltwater intrusion in a regional aquifer: Combining 3D saltwater modeling with geophysical and geochemical data. *Water Resources Research* 55(3), 1792-1813.
- MoE and UNDP (2011) State and trends of the Lebanese environment, Ministry of Environment, Beirut, Lebanon.
- MoEW and UNDP (2014) Assessment of groundwater resources of Lebanon, Ministry of Energy and Water, Beirut, Lebanon.
- Momejian, N., Abou Najm, M., Alameddine, I. and El-Fadel, M. (2019a) Can groundwater vulnerability models assess seawater intrusion? *Environmental Impact Assessment Review* 75, 13-26.
- Momejian, N., Abou Najm, M., Alameddine, I. and El-Fadel, M. (2019b) Groundwater Vulnerability Modeling to Assess Seawater Intrusion: a Methodological Comparison with Geospatial Interpolation. *Water Resources Management* 33(3), 1039-1052.

- Moran, P.A.P. (1948) The interpretation of statistical maps. *Journal of the Royal Statistical Society: Series B (Statistical Methodology)* 10(2), 243-251.
- Morgan, L.K., Bakker, M. and Werner, A.D. (2015) Occurrence of seawater intrusion overshoot. *Water Resources Research* 51(4), 1989-1999.
- Murgulet, D. and Tick, G. (2008) The extent of saltwater intrusion in southern Baldwin County, Alabama. *Environmental Geology* 55(6), 1235-1245.
- Naderi, M. (2020) Assessment of water security under climate change for the large watershed of Dorudzan Dam in southern Iran. *Hydrogeology Journal* 28, 1553–1574.
- Nash, J.E. and Sutcliffe, J.V. (1970) River flow forecasting through conceptual models part 1: a discussion of principles. *Journal of hydrology* 10(3), 282-290.
- Nishikawa, T., Siade, A.J., Reichard, E.G., Ponti, D.J., Canales, A.G. and Johnson, T.A. (2009) Stratigraphic controls on seawater intrusion and implications for groundwater management, Dominguez Gap area of Los Angeles, California, USA. *Hydrogeology Journal* 17(7), 1699-1725.
- Pebesma, E. (2018) Simple features for R: standardized support for spatial vector data. *The R Journal* 10(1), 439-446.
- Pebesma, E.J. (2004) Multivariable geostatistics in S: the gstat package. *Computers & Geosciences* 30(7), 683-691.
- Peltekian, A. (1980) Groundwater quality of greater Beirut in relation to geological structure and the extent of seawater intrusion, American University of Beirut, Beirut, Lebanon.
- Pitcock, J., Hussey, K. and Stone, A. (2016) *Integrated Groundwater Management: Concepts, Approaches, and Challenges*. Jakeman, A.J., Barreteau, O., Hunt, R.J., Rinaudo, J.-D. and Ross, A. (eds), pp. 75-96, Springer Open.
- R Core Team (2018) *R: A language and environment for statistical computing*, R Foundation for Statistical Computing, Vienna, Austria.
- Rachid, G. (2020) Managing seawater intrusion along data sparse coastal aquifers: a decision support tool based on a dynamic bayesian belief network, American University of Beirut, Beirut, Lebanon.
- RAMCO (2014) Residential prices in Beirut, the time for corrections, Beirut, Lebanon.

- Ranjan, P., Kazama, S. and Sawamoto, M. (2006) Effects of climate change on coastal fresh groundwater resources. *Global Environmental Change* 16(4), 388-399.
- Reilly, T.E. and Goodman, A.S. (1985) Quantitative analysis of saltwater-freshwater relationships in groundwater systems—a historical perspective. *Journal of Hydrology* 80(1), 125-160.
- Romanazzi, A., Gentile, F. and Polemio, M. (2015) Modelling and management of a Mediterranean karstic coastal aquifer under the effects of seawater intrusion and climate change. *Environmental Earth Sciences* 74(1), 115-128.
- Roson, R. and Damania, R. (2017) The macroeconomic impact of future water scarcity : an assessment of alternative scenarios. *Journal of Policy Modeling* 39(6), 1141-1162.
- Saadeh, M. (2008) Influence of overexploitation and seawater intrusion on the quality of groundwater in Greater Beirut, RWTH Aachen University, Aachen, Germany.
- Safi, A. (2019) Stochastic modeling of saltwater intrusion in highly heterogeneous coastal aquifers, American University of Beirut, Beirut, Lebanon.
- Sanford, W.E. and Pope, J.P. (2010) Current challenges using models to forecast seawater intrusion: lessons from the Eastern Shore of Virginia, USA. *Hydrogeology Journal* 18(1), 73-93.
- Sebben, M.L., Werner, A.D. and Graf, T. (2015) Seawater intrusion in fractured coastal aquifers: A preliminary numerical investigation using a fractured Henry problem. *Advances in water resources* 85, 93-108.
- Shi, L. and Jiao, J.J. (2014) Seawater intrusion and coastal aquifer management in China: a review. *Environmental Earth Sciences* 72(8), 2811-2819.
- Singh, A. (2014) Optimization modelling for seawater intrusion management. *Journal of Hydrology* 508, 43-52.
- Somayasa, W., Wibawa, G.A., Ruslan and Sutiari, D.K. (2019) Universal kriging of corn plant data under isotropic power type variogram model. *Journal of Physics: Conference Series* 1341(6).
- Taniguchi, M., Allen, D.M., Alley, W.M., VanderSteen, J., Gleeson, T., Sophocleous, M.A. and Zhou, Y. (2010) Groundwater sustainability strategies. *Nature Geoscience* 3(6), 378-379.
- Tomaszkiewicz, M., Abou Najm, M. and El-Fadel, M. (2014) Development of a groundwater quality index for seawater intrusion in coastal aquifers. *Environmental Modelling and Software* 57, 13-26.

Trabelsi, N., Triki, I., Hentati, I. and Zairi, M. (2016) Aquifer vulnerability and seawater intrusion risk using GALDIT, GQISWI and GIS: case of a coastal aquifer in Tunisia. *Environmental Earth Sciences* 75(8), 669.

Uddameri, V., Singaraju, S. and Hernandez, E.A. (2014) Impacts of sea-level rise and urbanization on groundwater availability and sustainability of coastal communities in semi-arid South Texas. *Environmental Earth Sciences* 71(6), 2503-2515.

UN (2012) *Managing water under uncertainty and risk*, UNESCO Paris, France.

USGS (2020) Landsat-8 image courtesy of the U.S. Geological Survey, United States Geological Survey, United States.

Ver Hoef, J.M. and Cressie, N. (1993) Multivariable spatial prediction. *Mathematical Geology* 25(2), 219-240.

Walley, C.D. (1997) The lithostratigraphy of Lebanon: a review. *Lebanese Science Bulletin* 10(1), 81-107.

Wang, M., Beelen, R., Eeftens, M., Meliefste, K., Hoek, G. and Brunekreef, B. (2012) Systematic evaluation of land use regression models for NO₂. *Environmental Science & Technology* 46(8), 4481-4489.

Watson, T.A., Werner, A.D. and Simmons, C.T. (2010) Transience of seawater intrusion in response to sea level rise. *Water Resources Research* 46(12).

Werner, A.D. (2010) A review of seawater intrusion and its management in Australia. *Hydrogeology Journal* 18(1), 281-285.

World Bank (2003) *Republic of Lebanon policy: note on irrigation sector sustainability*, Water, Environment, Social, and Rural Development Group: Middle East and North Africa Region and Agriculture and Rural Development Department, Washington, D.C.

Xiao, Y., Gu, X., Yin, S., Shao, J., Cui, Y., Zhang, Q. and Niu, Y. (2016) Geostatistical interpolation model selection based on ArcGIS and spatio-temporal variability analysis of groundwater level in piedmont plains, northwest China. *SpringerPlus* 5(1), 425.

Xu, H., Bechle, M.J., Wang, M., Szpiro, A.A., Vedal, S., Bai, Y. and Marshall, J.D. (2019) National PM_{2.5} and NO₂ exposure models for China based on land use regression, satellite measurements, and universal kriging. *Science of the Total Environment* 655, 423-433.

Young, M.T., Bechle, M.J., Sampson, P.D., Szpiro, A.A., Marshall, J.D., Sheppard, L. and Kaufman, J.D. (2016) Satellite-based NO₂ and model validation in a national

prediction model based on universal kriging and land-use regression. *Environmental Science & Technology* 50(7), 3686-3694.

Yu, X. and Michael, H.A. (2019) Mechanisms, configuration typology, and vulnerability of pumping-induced seawater intrusion in heterogeneous aquifers. *Advances in water resources* 128, 117-128.

Zalzal, J., Alameddine, I., El-Fadel, M., Weichenthal, S. and Hatzopoulou, M. (2020) Drivers of seasonal and annual air pollution exposure in a complex urban environment with multiple source contributions. *Environmental monitoring and assessment* 192(7).

Zekster, I. and Everett, L. (2004) *Groundwater resources of the world and their use*, UNESCO, Paris, France

Zhang, X., Liu, J., Tang, Y., Zhao, X., Yang, H., Gerbens-Leenes, P.W., . . . Yan, J. (2017) China's coal-fired power plants impose pressure on water resources. *Journal of Cleaner Production* 161, 1171-1179.